

Supporting Information

Ultra-low Pd loading nanocatalyst with high activity and stability for CO oxidative coupling to dimethyl oxalate

Si-Yan Peng,^{a,b} Zhong-Ning Xu,^{a,b} Qing-Song Chen,^{a,b} Yu-Min Chen,^{a,b} Jing Sun,^a
Zhi-Qiao Wang,^{a,b} Ming-Sheng Wang,^a Guo-Cong Guo^{a,*}

^a *State Key Laboratory of Structural Chemistry, Fujian Institute of Research on the Structure
of Matter, Chinese Academy of Sciences, Fuzhou, Fujian 350002, P. R. China*

^b *Key Laboratory of Coal to Ethylene Glycol and Its Related Technology, Chinese Academy
of Sciences, Fuzhou, Fujian 350002, P. R. China*

* *To whom correspondence should be addressed: E-mail: gcguo@fjirsm.ac.cn; Fax:*

+86-591-83714946; Tel: +86-591-83705882

1. Reactions of coal to ethylene glycol

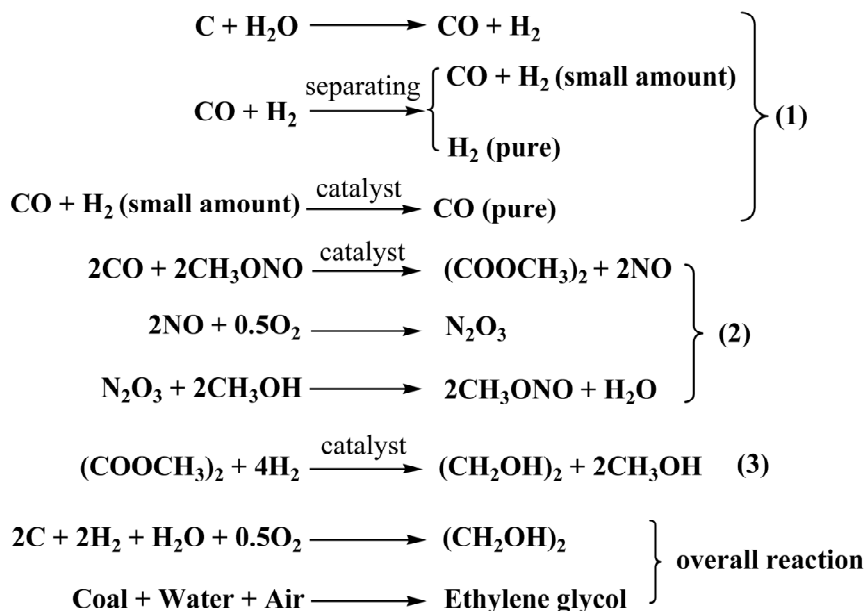


Figure S1. The reactions of coal to ethylene glycol.

Coal to ethylene glycol contains three main steps: 1) elimination small amount of hydrogen gas in CO separated from coal-derived synthesis gas; 2) CO oxidative coupling to DMO; 3) hydrogenation of DMO to ethylene glycol. The overall reaction means only coal, water and air are consumed to synthesize ethylene glycol, implying that coal to ethylene glycol is a green and atomic economy technology.

2. Photo of coal to ethylene glycol plant



Figure S2. The photo of the world's first set of 200 000 tons coal to ethylene glycol plant.

3. Experimental details

3.1 Materials

K_2PdCl_4 (AR; Sino-Platinum Co., Ltd., China); polyvinylpyrrolidone (PVP; Mw: ~30,000; BASF); $\text{CuCl}_2 \cdot 2\text{H}_2\text{O}$, $\text{Cu}(\text{NO}_3)_2 \cdot 3\text{H}_2\text{O}$, $\alpha\text{-Al}_2\text{O}_3$ and L-ascorbic acid (AR; Sino-Pharm Chemical Reagent Co., Ltd., China); citric acid (AR; Beijing Chemical Works, China). All chemicals were used as received without further purification.

3.2 Preparation of Pd/ $\alpha\text{-Al}_2\text{O}_3$ catalysts

Preparation of catalyst 1 (denoted as C1): Catalyst **C1** was prepared by a room-temperature, Cu^{2+} -assisted, in situ reduction method. K_2PdCl_4 (16.3 mg), $\text{CuCl}_2 \cdot 2\text{H}_2\text{O}$ (17 mg), PVP (222 mg), and citric acid (210 mg) were dissolved in 15 mL deionized water, and then 1 g $\alpha\text{-Al}_2\text{O}_3$ pre-calcined at 600 °C for 2 hours was dispersed into the solution with vigorous magnetic stirring at room temperature. After stirring for 30 minutes, a freshly prepared 5 mL aqueous solution containing 70 mg L-ascorbic acid was quickly added into the $\alpha\text{-Al}_2\text{O}_3$ slurry under magnetic stirring, and then the mixed slurry kept stirring for 16 hours at room temperature. The solid product was filtered, washed with deionized water and ethanol for several times, and dried at 60 °C for 8 hours under vacuum. Prior to the activity evaluation, the dried catalyst was treated under a flow of pure hydrogen at 400 °C for 3 hours.

Preparation of catalyst 2 (denoted as C2): Catalyst **C2** was prepared in the same preparation condition as **C1**, except that $\text{CuCl}_2 \cdot 2\text{H}_2\text{O}$ was not added.

3.3 Instrumentation

CO chemisorption: CO chemisorption was carried out on a Micromeritics AutoChem II 2920 with a thermal conductivity detector. The Pd specific surface areas and dispersions of catalysts were calculated from the amount of chemisorbed CO.

ICP: Inductively Coupled Plasma (ICP) elemental analysis measurements were carried out on an Ultima2 plasma emission spectrometer from Jobin Yvon.

XPS: X-ray photoelectron spectroscopy (XPS) measurements were performed with a VG Escalab 250 spectrometer equipped with an Al anode (Al-K α = 1486.7 eV). Samples in powder form were pressed into wafer for analysis.

XRD: Powder X-ray diffraction (XRD) patterns were measured on a glass wafer by a Rigaku MiniFlex II diffractometer with a Cu K α X ray source ($\lambda=1.5406 \text{ \AA}$) at scan speed of $3^\circ (2\theta)/\text{min}$. The X-ray tube was operated at 40 kV and 30 mA.

TEM: Samples for transmission electron microscopy (TEM) and high resolution TEM (HRTEM) observations were prepared by drying a drop of diluted ethanol dispersion of Pd/ α -Al₂O₃ nanocatalysts on copper grids. Images were obtained on a TEM (JEM-2010) operated at 200 kV.

In situ DR-FTIRS: In situ diffuse reflectance fourier transform infrared spectroscopy (DR-FTIRS) measurements were performed on a Nicolet 6700 diffuse reflectance infrared spectrometer equipped with a stainless steel in situ IR flow cell. The powder samples were placed into the cell and had been pretreated in Ar flow for 30 minutes at 423 K. After cooling down to the desired temperature, a reference spectrum was recorded. Then, the reactants were introduced in constant flowing and the spectra were recorded at a resolution of 4 cm^{-1} .

3.4 Evaluation of catalytic activity

The activities of the Pd/ α -Al₂O₃ nanocatalysts for CO oxidative coupling to DMO were carried out in a fixed-bed quartz tubular reactor. The Pd/ α -Al₂O₃ nanocatalysts (200 mg) were placed in the center of quartz tubular reactor. The reactant gases (28% CO, 20% CH₃ONO, 4% Ar and N₂ balance) were passed through the reactor at a gas hourly space velocity (GHSV)

of 3000 h^{-1} . The catalytic activity tests were performed in the temperature range of $90\text{--}150 \text{ }^\circ\text{C}$ under atmospheric pressure. The composition of the reactant gases and reaction products exiting the reactor was monitored by an on-line Shimadzu GC-2014 gas chromatography equipped with a thermal conductivity detector and a flame ionization detector.

The conversion of CO, the selectivity to DMO and the space-time yields (STY) of DMO were calculated using the following formulas:

$$\text{Conversion of CO (\%)} = (1 - ([\text{Ar}]_{\text{in}} / [\text{Ar}]_{\text{out}}) / ([\text{CO}]_{\text{in}} / [\text{CO}]_{\text{out}})) \times 100\%$$

$$\text{Selectivity to DMO (\%)} = (S_{\text{DMO}} \times R\text{-}F_{\text{DMO}}) / (S_{\text{DMO}} \times R\text{-}F_{\text{DMO}} + S_{\text{DMC}} \times R\text{-}F_{\text{DMC}}) \times 100\%$$

$$\text{STY of DMO (g}\cdot\text{L}^{-1}\text{h}^{-1}\text{)} = \text{Conversion of CO} \times \text{Selectivity to DMO} \times \text{GHSV of CO} \times 118.09 \text{ g}\cdot\text{mol}^{-1} / (2 \times 22.4 \text{ L}\cdot\text{mol}^{-1})$$

Where $[\text{Ar}]_{\text{in}}$ and $[\text{Ar}]_{\text{out}}$ are the concentration of Ar at the inlet and outlet, $[\text{CO}]_{\text{in}}$ and $[\text{CO}]_{\text{out}}$ are the concentration of CO at the inlet and outlet, respectively. S_{DMO} and S_{DMC} are the peak area of dimethyl oxalate and dimethyl carbonate, $R\text{-}F_{\text{DMO}}$ and $R\text{-}F_{\text{DMC}}$ are the relative correction factor of dimethyl oxalate and dimethyl carbonate, respectively.

4. Catalytic performance

4.1 GC chromatogram

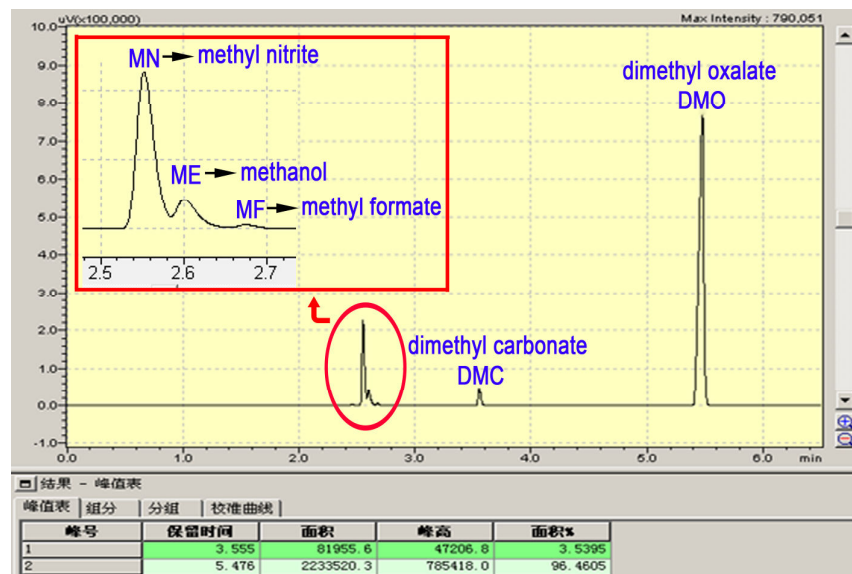
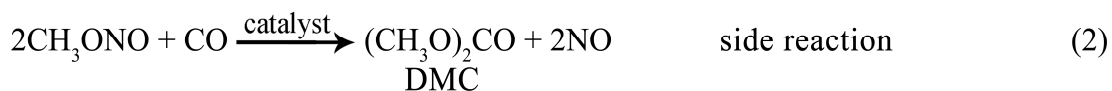
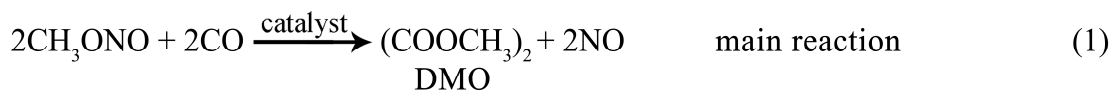


Figure S3. Gas chromatogram of the products from CO oxidative coupling to DMO on C1 at 130 °C.

Dimethyl oxalate (DMO) is our target product, and dimethyl carbonate (DMC) is the by-product in the CO oxidative coupling reactions. Very little methyl formate (MF) and methanol (ME) are identified. The characteristic peaks of MF and ME appear close to the reactant methyl nitrite (MN). However, MF and ME are produced from the catalytic decomposition of MN rather than the CO oxidative coupling reactions.¹ Herein, they do not influence the calculation of "selectivity to DMO" for CO oxidative coupling reactions.



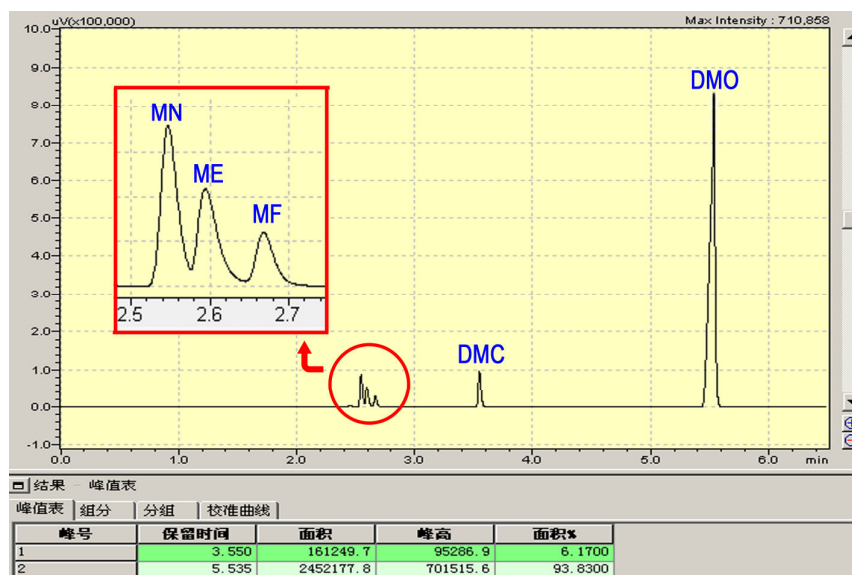


Figure S4. Gas chromatogram of the products from CO oxidative coupling to DMO on C1 at 150 °C.

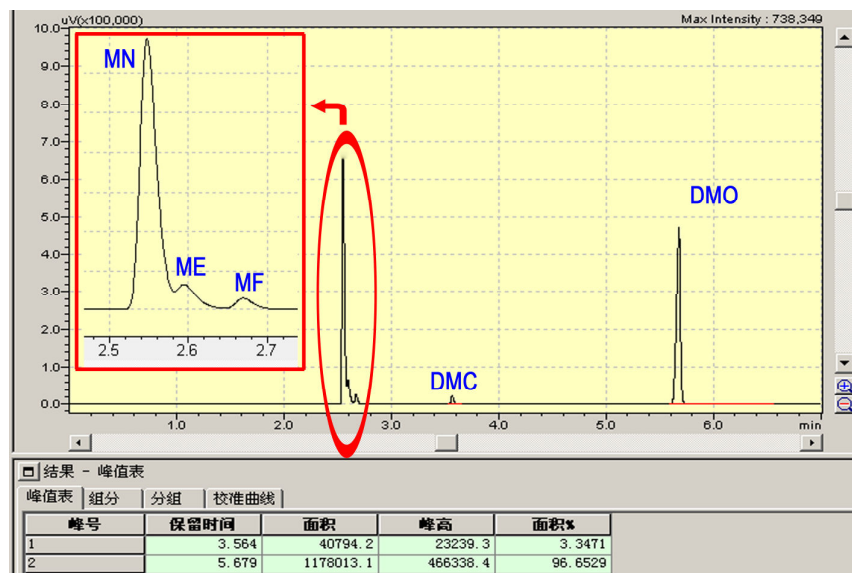


Figure S5. Gas chromatogram of the products from CO oxidative coupling to DMO on C2 at 130 °C.

Due to the chromatographic column efficiency varying in use, the peak retention times of the products also changed slightly.

4.2 Performances of catalysts with different Pd loadings

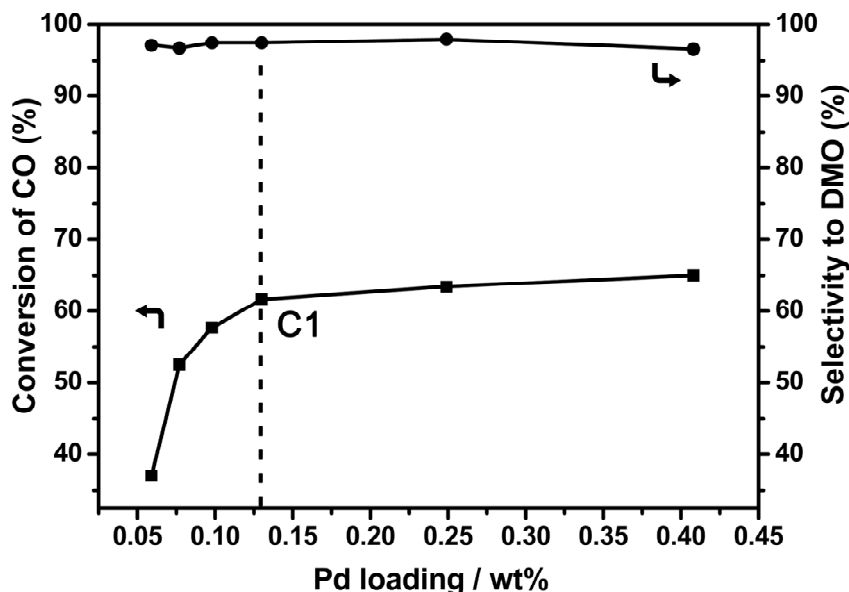


Figure S6. Conversion of CO (■) and selectivity to DMO (●) of as-synthesized catalysts with different Pd loadings for CO oxidative coupling to DMO at 130 °C. The catalysts were prepared with Cu²⁺-assisted synthesis method.

In order to investigate the influence of Pd loading on the CO oxidative coupling activity, we synthesized a series of catalysts with different Pd loadings, which were prepared with Cu²⁺-assisted synthesis method as **C1**. The catalysts with Pd loadings less than 0.13 wt% were prepared with the same method as **C1** by only varying the amount of α -Al₂O₃ support. The catalysts with 0.10 wt%, 0.08 wt%, and 0.06 wt% Pd loadings were obtained when the weight of added α -Al₂O₃ was 1.5 g, 2 g and 3 g, respectively. The preparation procedures for catalysts with Pd loadings higher than 0.13 wt% were similar to **C1**. The weight of α -Al₂O₃ support is 1g, while the amounts of other precursors (including water) were double and triple those of **C1** for preparing the catalysts with 0.25 wt% and 0.41 wt% Pd loadings, respectively.

According to Figure S6, when the Pd loading is lower than 0.13 wt%, the conversion of

CO increases dramatically with the rise of the Pd loading. However, we can see that when the Pd loading is higher than 0.13 wt%, it has little effect on the catalytic activity for CO oxidative coupling to DMO. This indicates that a Pd loading around 0.13 wt% is an optimal content from both catalytic performance and economical points of view.

5. Characterizations of catalysts

5.1 Pd loadings of catalysts

Table S1 The analysis on the difference of final Pd loadings between **C1** and **C2**

Catalysts	Theoretical Pd loading (wt%)	Final Pd loading (wt%)	Loss of Pd in the filtrate after reaction ^[a] (wt%)	Loss of Pd in the filtrate after washing ^[b] (wt%)
C1	0.53	0.13	0.31	0.06
C2	0.53	0.37	0.09	0.03

[a]: (weight of lost Pd in the filtrate after reaction)/(weight of α -Al₂O₃ support) × 100%.

[b]: (weight of lost Pd in the filtrate after washing)/(weight of α -Al₂O₃ support) × 100%.



Figure S7. The photo of the filtrates after reaction for preparing **C1** and **C2**

Table S1 shows the great difference on the final Pd loadings between **C1** and **C2** in spite that both catalysts have same theoretical initial Pd loading. It is obvious that the loss of Pd loading in **C1** is mainly from the filtrate after reaction. It arises from the effect of Cu^{2+} ions on the reduction process of PdCl_4^{2-} . The addition of Cu^{2+} ions into the reaction system inhibits the reduction of PdCl_4^{2-} precursor, resulting in the incomplete reduction. It should be pointed out that the loss of Pd in the filtrate after reaction can be reused.

According to the colour of the both filtrates after reaction (Figure S7), we can also easily infer that the PdCl_4^{2-} can be reduced incompletely by L-ascorbic acid in the presence of Cu^{2+} ions, and can be reduced nearly completely in the absence of Cu^{2+} ions.

5.2 XPS spectra of catalysts

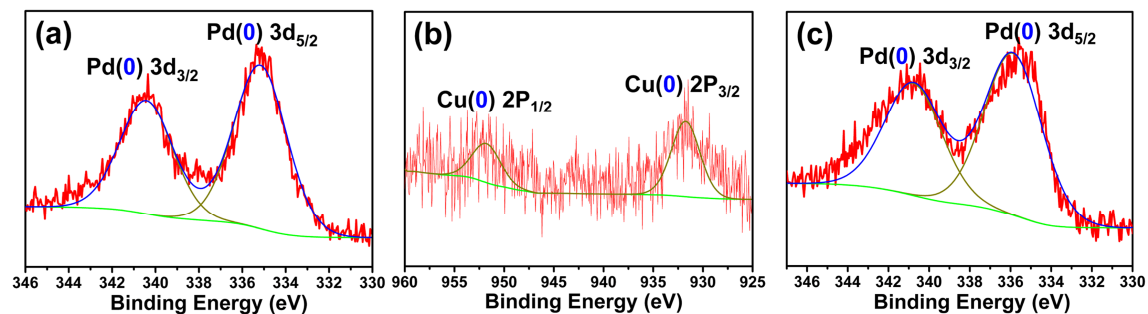


Figure S8. Pd 3d (a) and Cu 2p (b) XPS spectra of **C1** without H_2 treatment, and Pd 3d (c) XPS spectrum of **C2** without H_2 treatment, respectively.

5.3 XRD patterns

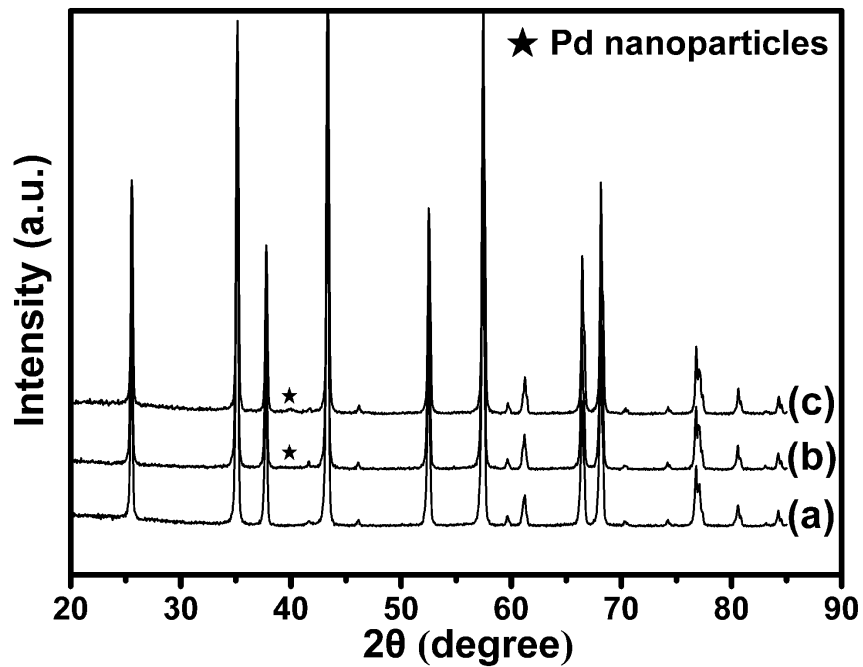


Figure S9. XRD patterns of α -Al₂O₃ (a), C1 (b) and C2 (c), respectively.

Both the XRD patterns of C1 and C2 are similar to that of α -Al₂O₃ support. The main diffraction peak corresponding to metallic palladium ($2\theta = 39.9^\circ$) was not detected, suggesting that the amount of Pd NPs is too small to be detected.

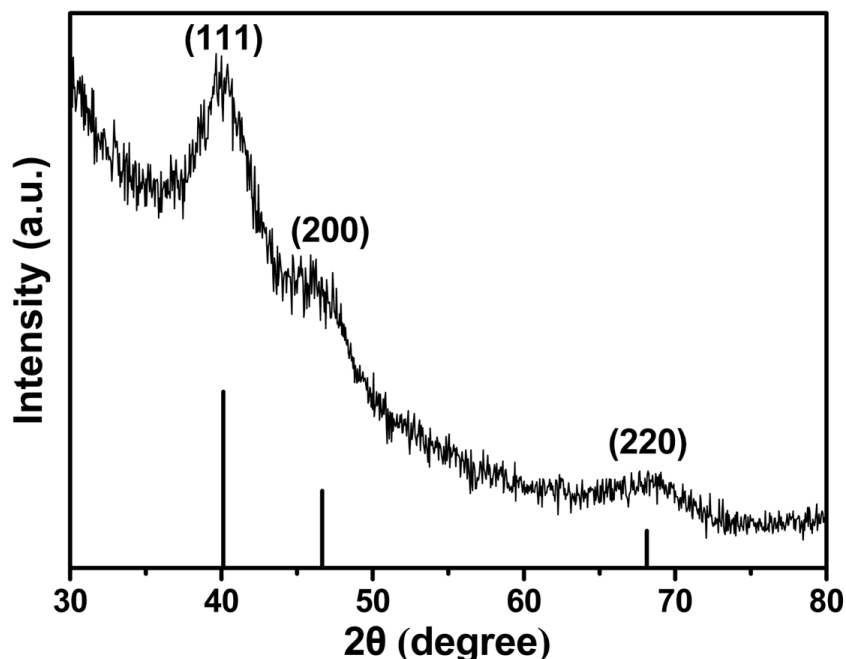


Figure S10. XRD pattern of as-synthesized Pd nanocrystals. The vertical lines indicate diffraction peaks of Pd face-centered cubic (fcc) phase (JCPDS 05-0681).

Although a trace amount of metallic state Cu did exist in **C1**, the nanoparticles of **C1** were Pd nanocrystals instead of Pd-Cu alloy. In order to confirm the phase structure of Pd nanocrystals more clearly, we synthesized a pot of Pd nanocrystals. The preparation procedures for Pd nanocrystals were same to **C1**, except that α -Al₂O₃ support was not added in the preparation. XRD pattern and TEM image of Pd nanocrystals are shown in Figure S10 and Figure S11, respectively. The three peaks located at 2θ values of ca. 40.0, 46.4, 68.2 ° can be assigned to (111), (200) and (220) characteristic diffractions, respectively, which represents the typical character of the face-centered cubic (fcc) Pd (JCPDS 05-0681). No diffraction peaks from Cu were detected. A similar phenomenon was also observed in the Cu²⁺-assisted synthesis of three-dimensional Pd polyhedron networks.² TEM image (Figure S11a) of as-synthesized Pd nanocrystals shows the average size of the Pd nanocrystals is 2.6 nm, which is close to the mean size of Pd NPs of **C1** (2.7 nm). The clear lattice spacing of the

HRTEM image (Figure S11b) taken from an individual nanoparticle is 0.226 nm, consistent with the (111) lattice spacing of the face-centered cubic (fcc) Pd. All these results demonstrate that the nanoparticles of **C1** were Pd nanocrystals instead of Pd-Cu alloy.

5.4 TEM and HRTEM images

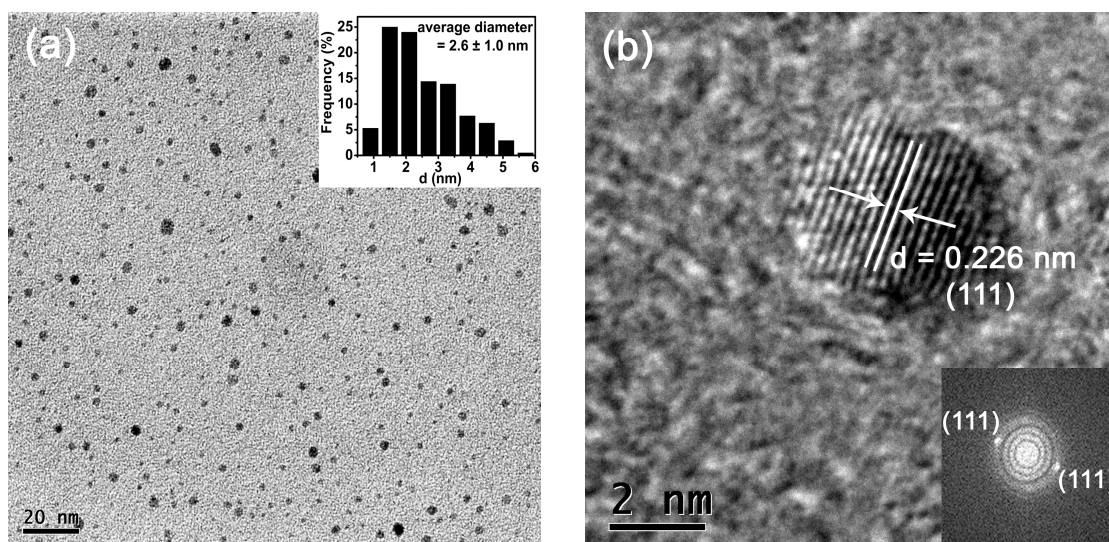


Figure S11. TEM image (a) and HRTEM image (b) of as-synthesized Pd nanocrystals. The inset of panel (a) shows the corresponding size distribution diagram. The inset of panel (b) shows the corresponding FFT pattern.

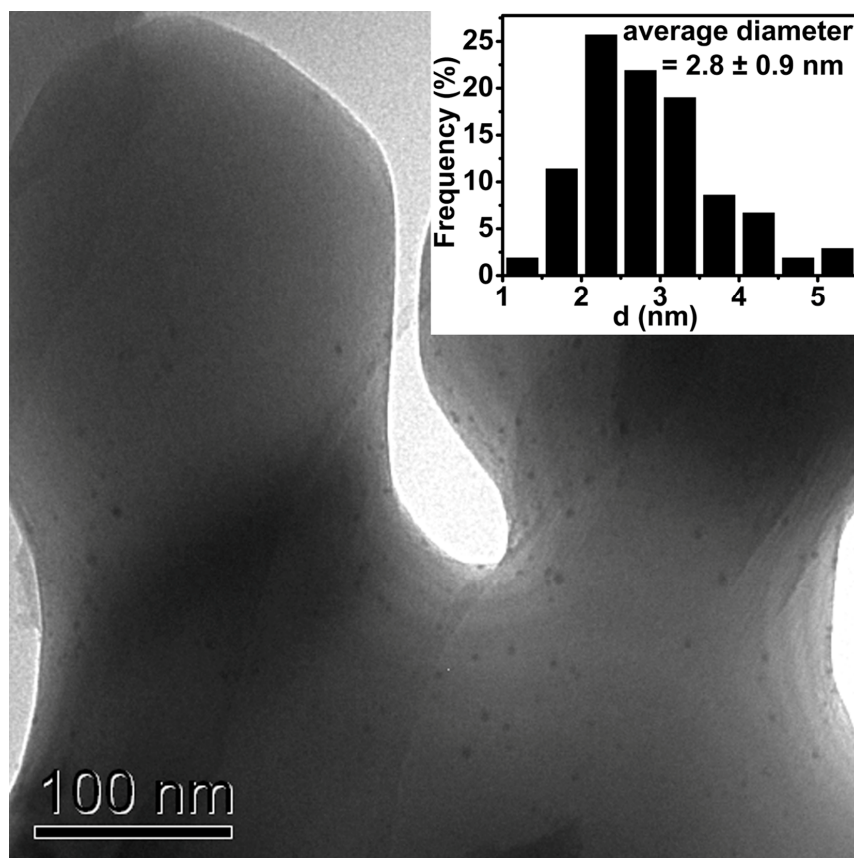


Figure S12. TEM image of **C1** after 100-h lifetime evaluation.

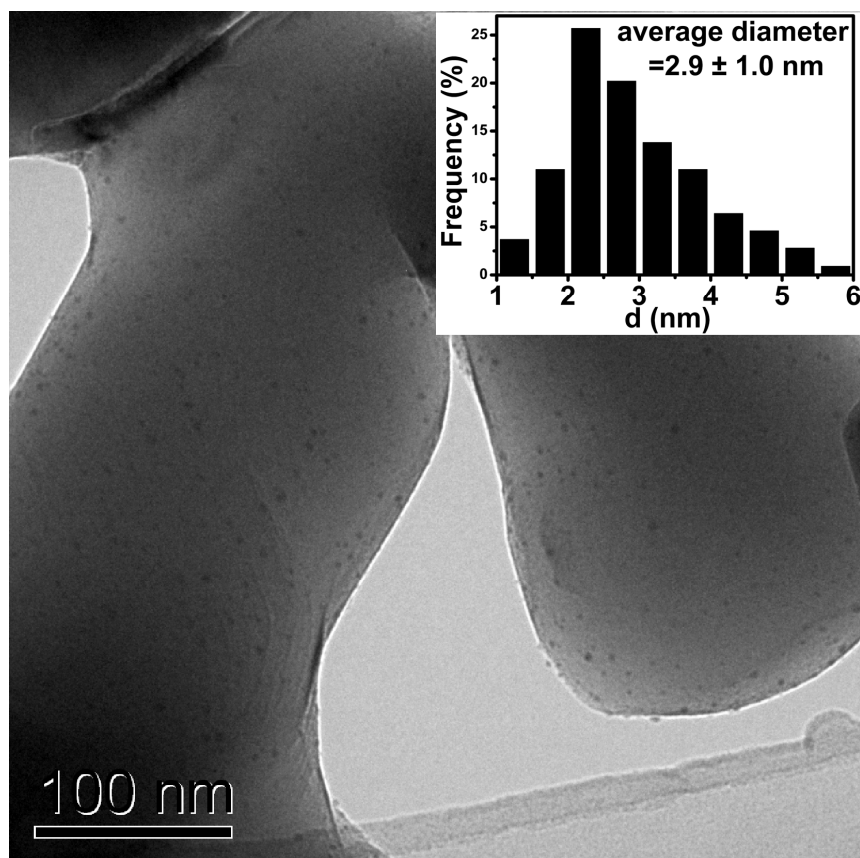


Figure S13. TEM image of the catalyst prepared with the addition of $\text{Cu}(\text{NO}_3)_2 \cdot 3\text{H}_2\text{O}$ instead of $\text{CuCl}_2 \cdot 2\text{H}_2\text{O}$.

6. References

- (1) G. L. Zhuo and X. Z. Jiang, *Catal. Lett.*, 2002, **80**, 171-174
- (2) Y. Xu, R. Xu, J. H. Cui, Y. Liu and B. Zhang, *Chem. Commun.*, 2012, **48**, 3881-3883